International Journal of Environmental Science and Technology (2023) 20:2745–2756
https://doi.org/10.1007/s13762-022-04138-3

ORIGINAL PAPER

Preparation of backfill materials by solidifying municipal solid waste incineration fly ash with slag-based cementitious materials

K. Wang[1,2,3] · K. Li[1,2,3] · X. Huang[1,2,3] · W. Ni[1,2,3] · S. Zhang[1,2,3]

Received: 22 February 2021 / Revised: 9 January 2022 / Accepted: 19 March 2022 / Published online: 9 April 2022

Abstract

In this study, solid waste granulated blast furnace slag and flue gas desulfurization gypsum were used to solidify municipal solid waste incineration fly ash to prepare cement-free backfill material. It was found that appropriate concentrations of fly ash (30 wt%) in backfill materials improved its mechanical strength, fluidity and rheological properties, as well as reducing the setting time, the ratio of bleeding and heavy metals leaching; shrinkage during drying was also restrained. XRD, FTIR and SEM results indicate that, under the action of OH^- in fly ash, depolymerization of surface alumina and silica structures of slag occurred, and a large volume of silicon-oxygen and aluminum-oxygen tetrahedra were released in the pore solution, forming $[Ca_2Al(OH)_6{\cdot}2H_2O]^+$. In sample M10, the hydration reaction of SO_4^{2-} from desulfurization gypsum and $[Ca_2Al(OH)_6{\cdot}2H_2O]^+$ resulted in the formation of ettringite due to the incorporation of insufficient fly ash. When the volume of fly ash increased, the alkaline environment improved the activity of the slag, the hydration reaction was favored by Cl^- from fly ash, and ettringite and Friedel's salt co-existed in the cementitious system. With a further increase in fly-ash content, almost all $[Ca_2Al(OH)_6{\cdot}2H_2O]^+$ released by slag reacted with Cl^- rather than SO_4^{2-} to produce Friedel's salt due to the small molecular size of Cl^-, which are more prone to react with $[Ca_2Al(OH)_6{\cdot}2H_2O]^+$, while ettringite disappeared. This study used solid waste to stabilize fly ash for the preparation of backfill material providing a new solution for fly-ash disposal, as well as providing an innovative method for low-cost and sustainable restoration of mine areas.

Keywords Municipal solid waste incineration fly ash · Cement-free · Backfill materials · Working performance · Friedel's salt · Ettringite

Abbreviations

MSW	Municipal solid waste
MSWI FA	Municipal solid waste incineration fly ash
GBFS	Granulated blast furnace slag
FGDG	Flue gas desulfurization gypsum

Editorial responsibility: Anna Grobelak.

✉ K. Li
Lkqing2003@163.com

[1] School of Civil and Resources Engineering, University of Science and Technology Beijing, Beijing 10083, China

[2] Key Laboratory of the Ministry of Education of China for High-Efficient Mining and Safety of Metal Mines, University of Science and Technology Beijing, Beijing 10083, China

[3] Beijing Key Laboratory of Resource-Oriented Treatment of Industrial Pollutants, University of Science and Technology Beijing, Beijing 10083, China

Introduction

With the rapid economic development in China, the production and storage of municipal solid waste (MSW) has rapidly increased. It was estimated that more than 260 million tons of MSW is generated in China each year, having an annual increase of about 8–10 wt%, resulting in seriously environmental degradation (Zhan et al. 2019). Incineration is an important method for removing municipal waste due to its many advantages, such as volume and weight reduction, fast processing speed and heat recycling (Hatami et al. 2021). After incineration of MSW, a certain amount of residue, including municipal solid waste incineration fly ash (MSWI FA) and bottom ash is generated, accounting for about 10–20% of the original waste weight. Bottom ash is the main residue from waste incineration, accounting for about 80% of the total residue. This ash consists of heterogeneous solid particles with a wide particle size distribution and different compositions, usually with a high silica and aluminum content and a low heavy metal content, resulting in its typical use

in the construction material sector (Tang et al. 2020; Tian et al. 2021; Šyc et al. 2020). However, as MSWI FA is collected in the flue gas purification system as well as in the heat recovery and utilization system, its yield is related to the type of waste, incineration conditions, incinerator type and flue gas treatment process. This waste generally accounts for about 3–5% of the total amount of incinerated waste (Bie et al. 2016b; Huang et al. 2017; Tan et al. 2013; Fan et al. 2021b; Tian et al. 2021). The types of MSW are very complex. During the incineration process, heavy metal elements in MSW will be migrated and transformed, and the majority of heavy metals are concentrated in the MSWI FA. This results in an extremely high heavy metal content in MSWI FA which can cause significant harm to soil, groundwater, air, the surrounding ecological environment and even human health. In addition, organic matter in MSW is incinerated to produce dioxins which are concentrated in MSWI FA. Dioxins are the collective name of 75 polychlorinated biphenyls and dioxins (polychlorinated dibenzo-p-dioxins, PCDDs) and 135 polychlorinated biphenyls and furans (polychlorinated dibenzofurans, PCDFs), 17 of which are strongly carcinogenic, teratogenic and mutagenic (Deng et al. 2020; He et al. 2022). In China, MSWI FA is classified as a hazardous waste, and it is stipulated in the *Technical specification for pollution control of fly ash from municipal solid waste incineration* (Chinese standard HJ 1134–2020) that this material can only be used as a resource after a harmless treatment.

Recently, solidification/stabilization (S/S) with various cements has been reported to be the optimal method to solidify MSWI FA; solidified materials are mainly used in mine backfilling (Wang et al. 2015; Zheng et al. 2019; Sobiecka 2013). However, the high price of cement has led to many limitations in mine backfill projects (Cihangir et al. 2012). In addition, the cement industry consumes a large number of raw materials, producing a large amount of CO_2. For example, production of a ton of Portland cement needs approximately 1.8 tons of raw material, producing about 1.0 ton of CO_2. Cement production is therefore detrimental to the environment, having limited ability to be used as an eco-efficient material (Zhang et al. 2011). Identifying new materials to replace cement for mine backfill is therefore important for the development of mine restoration (Clavier et al. 2019).

Granulated blast furnace slag (GBFS) is a solid waste obtained by quenching to a glassy state before crystallization during pig iron smelting. After grinding, GBFS has a potential hydraulic activity and chemical methods, involving the use of alkali and sulfate which can stimulate this activity. Although MSWI FA exhibits a certain cementitious activity, reactivity is relatively low and its inclusion may hinder the hydration reaction of cement (Igor et al. 2018). As MSWI FA is strongly alkaline, when it is used with flue gas desulfurization gypsum (FGDG), it can destroy the surface structure of GBFS, activating its potential activity to trigger a hydration reaction. The use of GBFS and FGDG as an alternative to cement to solidify MSWI FA is an efficient, cost-effective and sustainable strategy (Cihangir et al. 2012).

However, investigations have predominantly used GBFS as a binder for solidifying MSWI FA by adding an alkali-activator, such as geopolymer, metakaolin and cement to activate the activity of GBFS, thereby promoting the hydration reaction to achieve solidification (Lee et al. 2009; Long et al. 2021; Erfanimanesh and Sharbatdar 2020; Jin et al. 2016). Several studies have shown that needle-like ettringite and C–S–H gel were generated in alkali-activated-based materials, which in turn improved their workability and effectively sequestered the toxic substances in MSWIFA (Ren et al. 2021; Shao et al. 2021). This was an effective strategy to use MSWI FA and reduce heavy metal leaching, thereby reducing environmental pollution. Ettringite phase ($3CaO{\cdot}Al_2O_3{\cdot}3CaSO_4{\cdot}32H_2O$), also known as AFt, is a phase in which the $[Al(OH)_6]_3$ octahedra are linked through Ca^{2+} ions, forming columns along the c-axis of the needle axis (Behera et al. 2020; Liu et al. 2021). However, ettringite transforms into the AFm phase when there is an insufficient amount of S. AFm is regarded as material having a high Cl^- binding ability (Zhang et al. 2019a). A previous study has shown that tricalcium aluminate (C_3A) underwent a hydration step that led to the formation of the AFm structure ($[Ca_2Al(OH)_6{\cdot}2H_2O]^+$) (Liu et al. 2018). To balance the positive charge of the structure, Cl^- occupied the site above Al^{3+} in the space between the OH^- ions to form a Friedel's salt (Li et al. 2017; Zhou et al. 2017).

Research for this investigation was undertaken in 2019 in Beijing, China. Here, GBFS and FGDG were used to solidify MSWI FA, producing a backfill material. In the hydration reaction, alkaline substances in MSWI FA can activate the potential activity of GBFS to reduce the mobility of harmful substances in MSWI FA, thus reducing potential environmental degradation. As other alkali activator material is not added in this process, this method is more convenient. The effect of the MSWI FA content on the properties of backfill materials, such as water content of standard consistency, setting time, fluidity, mechanical strength, rheological properties, ratio of bleeding, drying shrinkage and leaching risk of heavy metals, was examined. Hydration product composition and morphology of pastes were studied using X-ray diffraction (XRD), scanning electron microscopy (SEM), and Fourier transform infrared spectroscopy (FTIR).

Materials and methods

Materials

MSWI FA used in this study was obtained from a MSW incineration plant in Beijing, China. The waste incinerator system used SN-type grate incineration technology from

the TAKUMA company in Japan. Incineration of MSW was performed between 850 and 1000 °C with a capacity of 1600 ton/day. Tailing and, GBFS and FGDG were collected from Hebei Xingtai Jintaicheng Environmental Resources Co., Ltd, China. Material was oven-dried at 35 °C for 72 h before being stored separately in a sealed bag for subsequent use. FGDG and GBFS were ground into a fine powder using a ball mill to increase its fineness for better reactivity.

Sample preparation

The mortar preparation method used in this study was based on the Chinese standard JGJ/T70-2009. After stirring, fresh mortar was immediately used for testing fluidity, rheological properties and ratio of bleeding. To assess the unconfined compressive strength and dry shrinkage of the specimens, homogeneous mortars were placed on a vibrating table to remove air bubbles and ensure a compact structure before being placed in 40 × 40 × 160 mm mold. After curing for 24 h in standard curing conditions (25 °C, 95% humidity), the molds were removed and samples were placed back in the curing box and sealed with a plastic film to avoid changes in water content and heavy metal leaching. The experimental conditions were selected to simulate the temperature and humidity of an underground mine in China (Li et al. 2020).

Samples used to understand hydration product composition and morphology of backfill material were stirred before the paste mixtures were placed in a 30 × 30 × 50 mm mold. Samples were removed after curing for 24 h. Curing continued for a further 28 days under the same conditions used for mortar samples. Samples were then broken and soaked in anhydrous ethanol for 48 h to stop the hydration reaction; samples were then dried in a vacuum oven at 35 °C for 72 h. Large samples were selected for SEM, while the remaining samples were finely ground (< 40 μm) and analyzed using XRD and FTIR.

The formulation of MSWI FA-slag-based backfill material is shown in Table S1. According to previous investigation (Wang et al. 2019), a total of eight different mixtures were prepared. The samples were denoted as Mx where x denotes the percent of mass of MSWI FA in the total mass of MSWI FA and binders (Table S1).

Experimental methods

Setting time test

The setting time test was carried out in accordance with the Chinese standard JGJ/T70-2009. The value of the penetration resistance was measured 2 h after curing and then measured every half hour until it reached 0.3 MPa. After this value had been reached, penetration resistance was then measured every 15 min until a value of 0.7 MPa was recorded. These two values are the initial setting time and the final setting time of the mortar, respectively.

Fluidity test

Mortar fluidity was measured in accordance with the Chinese standard GB/T 2419-2005. At the end of the experiment, mortar fluidity was calculated using average values (mm) of measured diameters of the slurry in two directions perpendicular to each other. Generally, gravity transportation occurs when fluidity exceeds 250 mm; fluidity of the slurry transported by the paste pump was recorded to be between 180 and 240 mm (Zhang et al. 2019b).

Mechanical strength and leaching test

The unconfined compressive strength test was measured in accordance with the Chinese standard GB/T17671-1999. In China, the strength of backfill material usually reaches 3 MPa after 28 days (Fan et al. 2018; Men and Xie 2018). The leaching test was performed according to the Chinese standard HJ 557-2010. After acidification, the concentration of heavy metals in the leachate was measured on a SHIMADZU 2030 inductively coupled plasma mass spectrometer (ICP-MS).

Ratio of bleeding

The experiment for ratio of bleeding was carried out in accordance with the Chinese standard JC/T 2153-2012. Fresh mortar was poured into a graduated cylinder and total mass was weighted (M_1). The mass of the graduated cylinder and water added to the mortar was denoted as M_g and M_2, respectively. After 30 min, slurry volume was observed every five minutes until a stable value was recorded, and the mass of the effluent water (M_3) was measured. The ratio of bleeding (Rb) was calculated as:

$$\mathrm{Rb} = \frac{M_3}{\left(M_1 - M_g\right) \times (M_2 \times 100)/(M_2 + 1800)} \times 100 \quad (1)$$

Dry shrinkage test

The drying shrinkage test was carried out in accordance with the Chinese standard JGJ/T70-2009. Mortar was placed into test molds, compacted and then placed in a curing room at 20 ± 5 °C. After 7 days, the molds were removed and initial lengths measured; directions were marked on the mortar.

Specimen lengths were measured according to the marked direction after 7, 14, 21, 28, 56 and 90 days.

Rheological properties

In the absence of a standard for the measurement of rheological properties of mortar, convenient methods for sample pre-treatment and testing were developed. Prior to each measurement, samples were stirred with a spatula for 1 min to obtain a homogeneous mixture. Stirring was performed to limit any effect of self-settlement of the tailing particles during curing, as well as to break bonds generated by hydration products. The stirring blade was then gently inserted into the mortar, and the minimum depth of the mortar was equal to twice the height of the stirring blade. A motor was turned on and the internal structure of the mortar was continuously damaged, creating a shear stress on the rotor. The shear rate of the rotor increased from 0 to 120 Pa/s in 120 s, and shear stress was recorded (Jiang et al. 2019). Shear stress generated at different shear rates was used to understand the relationship between internal stresses and the dynamic equations in the mold evolution. Finally, shear yield stress and plastic viscosity were calculated, and the type of fluid of the mortars was determined (Nguyen and Boger 1985; Petra and David 1996; Jiang et al. 2016).

Results and discussion

Raw materials

After grinding or drying treatment, the specific surface areas of MSWI FA, GBFS and FGDG were 340, 500 and 450 m^2/kg, respectively (analyzed by CZB-9 BET Automatic Specific Surface Area Analyzer). Particle size of the raw materials was analyzed using a LMS-30 laser diffraction scattering particle size distribution analyzer (Fig. S1). Volume accumulative distribution (VAD) of 10, 50 and 90% of the different raw materials is displayed on the upper left corner of the particle size distribution. XRF test results (analyzed by XRF-1800 sequential X-ray fluorescence spectrometer) of raw materials are shown in Table S2. XRD spectra (Fig. S2) were recorded using a Rigaku D/Max-RB X-ray diffractometer in the range of 5°–90°.

Tailing sand

The main chemical elements in the tailing sand were Ca, Si, Mg, Al and Fe (Table S2), and the main mineral phases of tailing sand were SiO_2 and a small amount of $CaCO_3$ (Fig. S2a).

GBFS

The main chemical elements in GBFS were Ca, Si, Mg and Al (Table S2). Figure S2b shows the XRD pattern of GBFS, displaying an obvious broad band, which indicates the predominant amorphous nature of the GBFS. In addition, a small contribution of crystalline $CaCO_3$ was observed. According to the Chinese National Standard for Granulated blast-furnace slag used for cement production (GB/T 203-2008), the performance indices of GBFS were calculated based on its chemical composition and by applying Eqs. (2)–(4). It can be seen that GBFS used in this study is a high-quality slag with high activity and neutral alkalinity.

Hydraulic activity

$$K = w(CaO + MgO + Al_2O_3)/w(SiO_2) = 2.23 > 1.6 \quad \text{(High quality)} \tag{2}$$

Activity coefficient

$$H_0 = w(Al_2O_3)/w(SiO_2) = 0.50 > 0.25 \quad \text{(High activity)} \tag{3}$$

Alkalinity coefficient

$$M_0 = w(CaO + MgO)/w(SiO_2 + Al_2O_3) = 1.15 > 1 \quad \text{(Alkalinity)} \tag{4}$$

where W represents the mass fraction.

FGDG

FGDG used in this study is the main by-product of the wet limestone-gypsum desulfurization process. The main chemical elements in FGDG are Ca and S, while the main mineral phase is $CaSO_4{\cdot}2H_2O$ (arrow in Fig. S2c).

MSWI FA

The main chemical elements in MSWI FA are Ca, Cl, S, Na and K, whereas the main mineral phases are NaCl, KCl, $CaSO_4$, $CaCO_3$ and $Ca(OH)_2$. The concentration of each PCDD/Fs (polychlorinated dibenzo-p-dioxins and dibenzofurans) congener of MSWI FA was recorded to be notably lower than those of the relevant standard (Table S3). This investigation therefore mainly focused on controlling heavy metal leaching.

Effect of the MSWI FA content on the mortar performance

Water content of standard consistency and setting time

Water content of standard consistency (represented by WCSC in Fig. 1) of the backfill material tended to initially

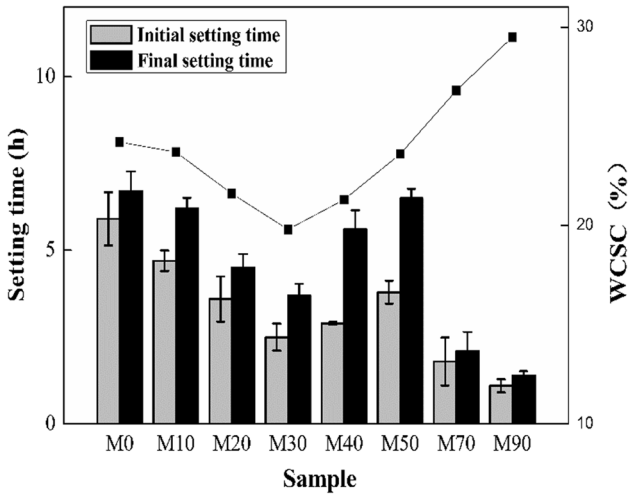

Fig. 1 Effect of MSWI FA content on mortar setting time

decrease before increasing with an increase of MSWI FA inclusion. Water content of standard consistency of sample M0 was 24.2%, while those of samples M10, M20 and M30 were reduced by 0.5%, 2.6% and 4.4%, respectively. These changes were due to the specific surface area of MSWI FA being smaller than that of GBFS. The incorporation of MSWI FA reduced the overall fineness of the cementitious material, and the reduction of the proportion of fine particles reduced the water adsorption capacity and water consumption of backfill materials. Standard consistency water consumption was recorded to gradually increase for samples M40, M50, M70 and M90. In samples M40 and M50, strong water absorption by MSWI FA accounted for the gradual increase in water content. Further inclusion of MSWI FA increased water absorption of the cementitious system, among which the water content of standard consistency of samples M70 and M90 significantly increased, reaching 26.8% and 29.5%, respectively.

The effect of MSWI FA amount on mortar setting time (Fig. 1) was examined. Initial (11.8 h) and final (13.5 h) setting times of M0 were recorded to be the longest out of all samples. With an increase in MSWI FA incorporation, sample setting time decreased accordingly, and for sample M50, initial and final setting times were 7.7 and 9.1 h, respectively. However, the tendency to decrease was very obvious for samples M70 and M90; initial and final setting times for sample M90 were 2.1 and 2.3 h, respectively.

For sample M0, the absence of MSWI FA led to incomplete activation of GBFS, resulting in a weak hydration reaction and long setting time of the cementitious system. When MSWI FA was added to the system, the system became alkaline and potential activity of GBFS was promoted. As a result, the release of $[Ca_2Al(OH)_6{\cdot}2H_2O]^+$ from GBFS and hydration of SO_4^{2-} ions in FGDG and Cl^- ions in MSWI FA with $[Ca_2Al(OH)_6{\cdot}2H_2O]^+$ occurred, accelerating the speed of hydration reaction and shortening mortar setting time. However, initial and final setting times drastically increased as MSWI FA content further increased. This is due to the fact that although the increase in heavy metal content and reduction of active components in mortar led to scarce hydration reaction (Bie et al. 2016a), strong water absorption of MSWI FA resulted in rapid mortar sticking. This process formed a highly viscous mud which significantly decreased initial and final setting times (Fig. 1).

Fluidity, leaching and mechanical strength

Fluidity and mechanical strength of the backfill material are essential parameters for successful transportation and a safe underground working environment for all mining personnel. Heavy metal leaching concentration determines the environmental safety of the backfill material. In this work, the effect of MSWI FA on strength and fluidity of the backfill material was studied (Fig. 2). Mechanical strength of the backfill material was recorded to initially increase before decreasing as the amount of MSWI FA incorporation increased (Fig. 2). For sample M0, when no MSWI FA was incorporated, the mechanical strength of the backfill material was only 5.49 MPa after 360 days, mechanical strength increased with an increase in MSWI FA, reaching 29.06 MPa (the highest value) in sample M30. After M30, further increases in MSWI FA resulted in dramatic decreases in mechanical strength of the backfill material. Hence, mechanical strength of samples M70 and M90 was less than 3 MPa after 360 days. This result is due to the fact that when the backfill materials are not modified with MSWI FA, GBFS activity cannot be fully activated only by SO_4^{2-} in FGDG, resulting in an insufficient hydration

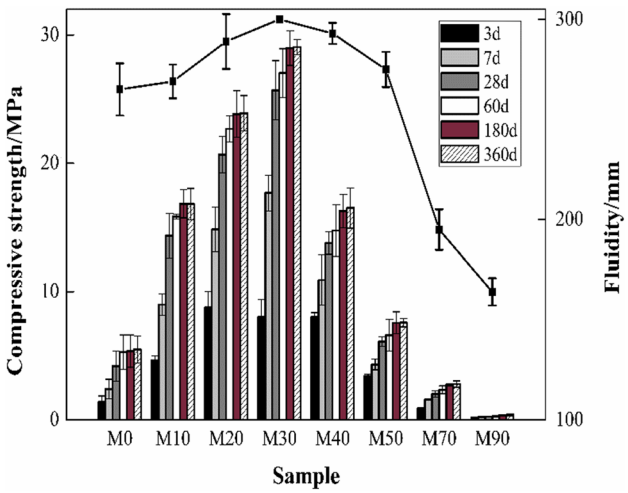

Fig. 2 Fluidity and mechanical strength in mortar samples

reaction which leads to a poor strength of the backfill materials. However, for samples M10, M20 and M30, incorporation of WSWI FA acts as an alkali activator and the activity of GBFS was gradually stimulated, resulting in an improvement in the rate of the hydration reaction and the internal stability of the mortar (Fan et al. 2021a; Liu et al. 2021). In addition, a large number of hydration products and a dense structure were formed which improved the strength and working performance of the backfill material. When MSWI FA content further increased due to the low cementitious ability of MSWI FA, the contribution of active components in the cementitious system was lower. The hydration reaction was therefore weak as only a few hydration products were generated, thereby decreasing the mechanical strength.

In addition, as the amount of MSWI FA increased, fluidity initially increased 300 mm before decreasing. This change was due to the fact that the particle size of MSWI FA was in between GBFS, FGDG and tailing sand, and a small amount of MSWI FA can improve the particle size distribution of the backfill material; MSWI FA particles are mainly in the form of regular spherical, which have the role of ball-bearings and lubrication, thereby improving fluidity of fresh mortar. However, MSWI FA has a strong water absorption ability, leading to a decreased in the amount of free water, thereby reducing fluidity.

The results of leaching of heavy metals after a curing treatment of 28 days are shown in Table 1. According to the standard for groundwater quality in China (GB/T 14848-2017), the concentration of heavy metals in MSWI FA was recorded to be higher than the environmental safety limits. It is worth noting that the concentration of all leaching heavy metals in backfill materials increased with an increase in the amount of MSWI FA; however, they were lower than the values in the relevant safety regulations. Immobilization efficiency for all heavy metals was recorded to be > 95%.

These results indicate that the GBFS and FGDG blended with MSWI FA as backfill material met the regulations for strength and fluidity in mine backfill. Hydration products in harden mortar could effectively immobilize the heavy metals, resulting in a safe range for heavy metal leaching.

Drying shrinkage

The hydration reaction and continuous evaporation of water from mortars resulted in shrinkage. Shrinkage stress generated during the shrinkage process caused cracks in the mortar, which reduced mechanical properties and durability (Yu et al. 2021). According to experimental results discussed above, samples M70 and M90 had poor working performance, and mechanical strength did not meet mine backfill regulations. Therefore, drying shrinkage was only evaluated for samples M0–M50. The effect of MSWI FA on drying shrinkage at different curing times was also investigated (Fig. 3). Results indicate that an increase in curing time led to an increase in dry shrinkage due to the hydration reaction and water lost through evaporation. The results also show that sample shrinkage was basically stable after 28 days, due to completion of the hydration reaction, the number of hydration products and evaporated water tend to be balanced.

Potential activity of GBFS in samples M0 and M10 was inadequately stimulated due to insufficient MSWI FA incorporation (Fig. 3), which in turn decreased the amount of hydration products, resulting in a low rate of shrinkage. The increase in MSWI FA content is favorable for shrinkage because the potential activity of GBFS was gradually activated and hydration of the cementitious system was strengthened. These changes resulted in a decrease in the overall specific surface area of the cementitious system and an increase in sample pore structure, leading to a reduction

Table 1 Leaching test results for M0-M90 (mg/kg)

Sample	Cu	Zn	Pb	Cd	As	Ni	Cr
MSWI FA	2914.36	543.48	253.10	87.19	35.47	223.84	457.26
M0	0.28	1.59	0.17	0.07	0.23	1.71	1.90
M10	0.87	2.35	1.22	0.61	1.33	2.33	4.69
M20	1.02	5.68	1.57	1.26	1.55	3.66	9.77
M30	2.29	11.17	2.89	2.05	2.18	3.92	13.94
M40	2.66	11.26	3.33	2.51	2.92	4.32	18.52
M50	5.12	15.64	3.56	3.09	4.29	5.59	27.99
M70	8.34	19.27	5.15	3.81	5.60	7.03	38.55
M90	16.92	31.89	7.24	4.09	5.90	9.01	44.11
GB/T 14,848–2017	1000	1000	10	5	10	20	50
Average Ie (%)*	98.23	97.41	99.30	99.10	99.03	97.73	95.15

**Ie* immobilization efficiency

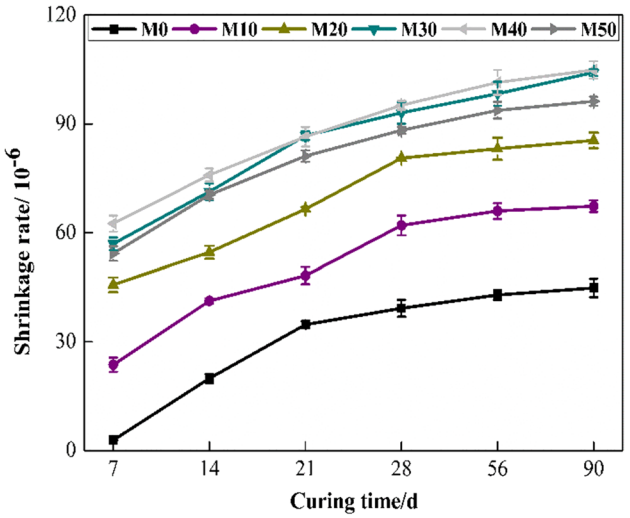

Fig. 3 MSWI FA content effect on dry shrinkage of backfill materials

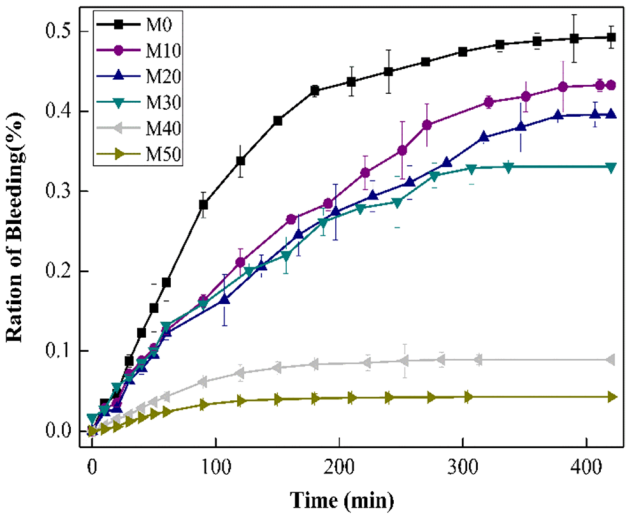

Fig. 4 MSWI FA content effect on the ratio of bleeding of backfill material

in total sample volume. Sample M50 recorded strong water absorption of MSWI FA which led to a decrease in the amount of free water in the cementitious system. This in turn decreased the mass ratio of water to cementitious material, reducing the drying shrinkage (You et al. 2020).

Ratio of bleeding

Bleeding is a phenomenon whereby some water moves from inside of the slurry to the surface during the standing process after the slurry has been well stirred. This phenomenon is unavoidable during backfill material preparation. An excessive ratio of bleeding will result in structural and textural defects of the backfill material (Ghourchian et al. 2016). Controlling the ratio of bleeding of the backfill material is therefore very important to ensure its working performance. The impact of MSWI FA content on the ratio of bleeding of backfill material is shown in Fig. 4.

The ratio of bleeding for samples M0-M30 gradually decreased, and time taken to reach a steady state reduced from 420 to 377 min. Combined with setting time experiment results, this indicates that acceleration of hydration reaction process due to blending a certain amount of MSWI resulted in mortar cohesion and homogeneity. This reduced the separation degree between the cementitious components and water, thereby reducing the ratio of bleeding. In samples M40 and M50, the degree of hydration reaction was very weak due to the presence of only a few active components producing a low amount of hydration products, resulting in a loose structure. However, due to strong water absorption of the MSWI FA, mortars were viscous with a small loss of free water. This is associated with a ratio of bleeding less than 0.1%, and the time needed for samples M40 and M50 to reach equilibrium sharply decreased to 253 and 150 min, respectively.

Rheological properties

Rheological property results for samples M0-M50 indicated that an increase in rotation speed resulted in a gradual increase in shear stress of the rotor; mortar shear stress increased with increasing MSWI FA content (Fig. 5). For sample M0, the low activation of the potential activity of GBFS led to a weak hydration reaction and few hydration products, which in turn led to a loose structure. As a result, mortar had a low yield

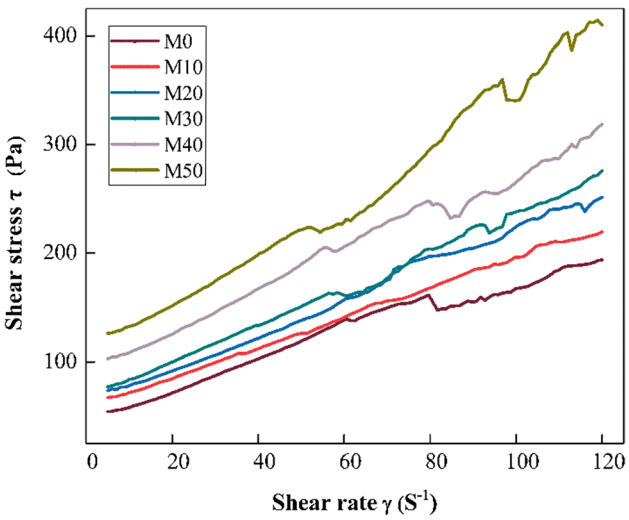

Fig. 5 Effect of the MSWI FA content on the rheological properties of backfill material

stress and plastic viscosity, as well as low resistance to the rotor. For samples M10–M40, the increase in MSWI FA content increased alkalinity of the mortar system, resulting in gradual depolymerization of the GBFS surface which greatly activated its potential activity. Hence, the hydration reaction was greatly stimulated, resulting in an increased contribution of hydration products. As a result, internal mortar structure became compact and yield stress and plastic viscosity were enhanced, improving the rotor resistance. For sample M50, strong water absorption of MSWI FA increased mortar viscosity, thereby notably increasing rotor resistance and shear stress.

By comparing shear rates and shear stresses of different MSWI FA blended mortar, curves for all samples were found to have an almost-straight line; thus, the fluid type of the backfill material was determined to be a Bingham's fluid. In a Bingham fluid, rheological properties are calculated with an equation containing two parameters, i.e., yield stress and plastic viscosity (Eq. 5). The simulation of rheological parameters for all samples is shown in Table 2.

$$\tau = \tau_0 + \eta_{pl}\gamma \tag{5}$$

where τ is shear stress (Pa); τ_0 is shear yield stress (Pa); η_{pl} is plastic viscosity (Pa·S); and γ is Shear rate (S^{-1}).

Table 2 Rheological parameter simulation results

Rheological parameter	η_{pl}	τ_0	R^2
M0	1.21	53.02	0.97143
M10	1.38	57.84	0.99886
M20	1.63	59.16	0.99585
M30	1.70	64.99	0.99618
M40	1.80	94.02	0.98931
M50	2.58	94.86	0.98237

As shown in Table 2, plastic viscosity of sample M0 was 1.21 Pa·s, and plastic viscosity of backfill slurry gradually increased with the incorporation of MSWI FA. Compared to sample M0, plastic viscosities of samples M10–M40 were 1.38 Pa·s, 1.63 Pa·s, 1.70 Pa·s and 1.80 Pa·s, recording increases of 14.0%, 34.7%, 40.5% and 48.8%, respectively. These results indicated that the incorporation of MSWI FA promoted a hydration reaction, and the filling effect of hydration products enhanced the internal friction between solid particles, solid and liquid phases, and liquid phases of the backfill slurry, which in turn increased its viscosity. Plastic viscosity of sample M50 significantly increased to 2.58 Pa·s, which was 113.2% higher than that of sample M0. This result is consistent with shear stress results in the rheological performance test. This is due to the strong water absorption of MSWI FA, which led to a reduction in free water in sample M50. A substantial increase in friction of internal components resulted in a significant increase in plastic viscosity of the backfill slurry.

Hydration characteristics

As samples M10–M40 recorded optimal working ability, they were used to study hydration characteristics.

XRD

XRD analysis was used to examine crystalline phases of the samples. Diffractograms for the samples are shown in Fig. 6.

Under the action of OH^- in MSWI FA, depolymerization of surface alumina and silica structures of GBFS occurred, and a large amount of silicon-oxygen and aluminum-oxygen tetrahedra were released in the pore solution, forming $[Ca_2Al(OH)_6{\cdot}2H_2O]^+$. This compound reacts with the SO_4^{2-} to produce AFt or adsorbs chloride to form a Friedel's

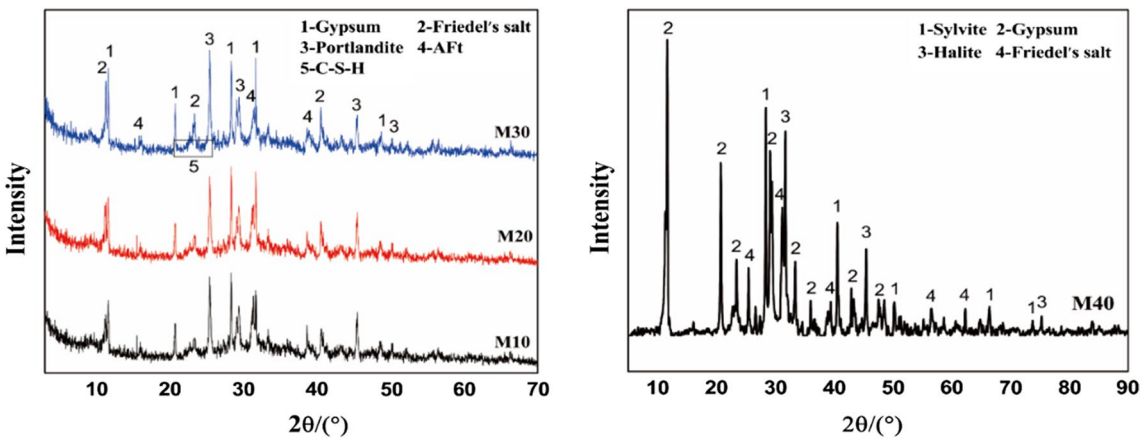

Fig. 6 XRD patterns of samples

salt (Shi et al. 2017; Ren and Ling 2021), as shown in Eqs. (6) and (7).

$$2Ca(OH)_2 + 3CaSO_4 \cdot 2H_2O + Al_2O_3 + 23H_2O \rightarrow 3CaO \cdot Al_2O_3 \cdot 3CaSO_4 \cdot 32H_2O \quad (AFt) \tag{6}$$

$$2Ca(OH)_2 + CaCl_2 + Al_2O_3 + H_2O \rightarrow 3CaO \cdot Al_2O_3 \cdot CaCl_2 \cdot 10H_2O \quad (\text{Friedel's salt}) \tag{7}$$

XRD results indicated that sample M10 is mainly formed of ettringite (AFt) as the hydration product due to the low Cl^- content (Fig. 6). However, due to weak alkaline conditions in the cementitious system, activation of GBFS was weak, the amount of ettringite was small, and a large proportion of unreacted $CaSO_4{\cdot}2H_2O$ and an amorphous phase in GBFS were identified. Samples M20 and M30 recorded an increase in the ratio of Cl^-/SO_4^{2-}, and transformation of AFm into Friedel's salt was obvious. This was confirmed by an increase in intensity of the corresponding XRD peaks. The AFm phase containing both Cl^- and SO_4^{2-} could also be formed, as shown in Eq. (8).

$$4Ca^{2+} + 2Al(OH)_4^- + SO_4^{2-} + Cl^- + xSO_4^{2-} + 4OH^- + 6H_2O \rightarrow 3CaO \cdot Al_2O_3 \cdot xCaSO_4 \cdot 0.5(1-x)CaCl_2 \cdot 12H_2O \quad (0 < x < 1) \tag{8}$$

Owing to the small molecular size, Cl^- can react with $[Ca_2Al(OH)_6{\cdot}2H_2O]^+$ before SO_4^{2-}. In sample M30, when the solution had a sufficient concentration of Cl^-, chloride-calcium aluminate phase (Friedel's salt) was formed earlier than the sulfate–calcium aluminate phase (ettringite). According to the study from Wan et al. (2018), ettringite is only formed when the amount of MSWI FA is < 10%. This occurrence explains the formation of Friedel's salt instead of ettringite as the main hydration product in the sample M30, as observed in the XRD pattern. In sample M40, however, unreacted KCl and NaCl in the MSWI FA were identified due to saturation of Cl^- that could participate in the hydration reaction. According to XRD results, the increase in MSWI FA content was favorable for the formation of hydration products which filled the pores of the samples. This occurrence was supported by an increase in mortar strength.

FTIR

FTIR spectra of samples M10–M40 display vibration bands depending on their chemical composition (Fig. 7). The band at 3413.49 cm^{-1} was attributed to asymmetric stretching vibration of physisorbed H_2O, and the band near 1620 cm^{-1} was assigned to the bending vibration of lattice water. These findings indicate that a product containing crystal water was produced during the hydration reaction. The band near 1435 cm^{-1} may derive from a small amount

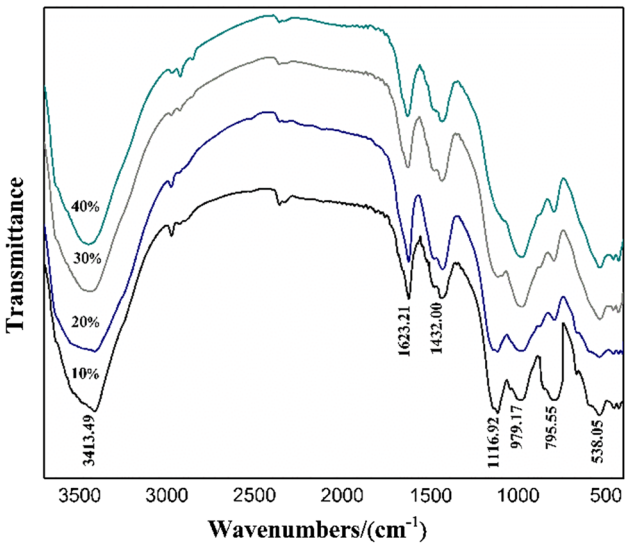

Fig. 7 FTIR analysis of samples

of CO_3^{2-} generated by the reaction with CO_2 in air during hydration. The band at 1117 cm^{-1} was attributed to the stretching vibration of S–O in sulfate ions, indicating the formation of ettringite during the hydration reaction. The incorporation of MSWI FA resulted in the decrease in intensity of this band, proving a decrease in ettringite content. This result is in accordance with XRD results. Bands at 979 and 560 cm^{-1} confirmed the presence of Al–OH and $[AlO_6]$ octahedrons, respectively, indicating the formation of ettringite and Friedel's salt during the hydration reaction. The band around 795 cm^{-1} belongs to Si–O in the C–S–H gel, although its intensity indicates the formation of a low amount of C–S–H gel, consistent with XRD results.

SEM

SEM images from samples M10–M40 are shown in Fig. 8. As shown in Fig. 8a, ettringite (A) was the main hydration product in the cementitious system in sample M10 due to the presence of few Cl^- ions from raw materials. However, due to weak hydration, the amount of ettringite was very small. Sample M20 contained a higher amount of MSWI FA (arrow in Fig. 8b), thereby favoring the hydration reaction: two phases co-exist in the cementitious system (ettringite and Friedel's salt; B), a finding that is in agreement with XRD results. In sample M30, GBFS was fully activated. The cementitious system contained a large amount of Cl^-, enough to consume $[Ca_2Al(OH)_6{\cdot}2H_2O]^+$ released by GBFS, producing a large amount of Friedel's salt. In addition, ettringite gradually disappeared during the hydration reaction. Morphology of Friedel's salt was a hexagonal slice with a size between 2 and 3 mm. According to the image displayed in Fig. 8c, a small amount of C–S–H gel (C) can

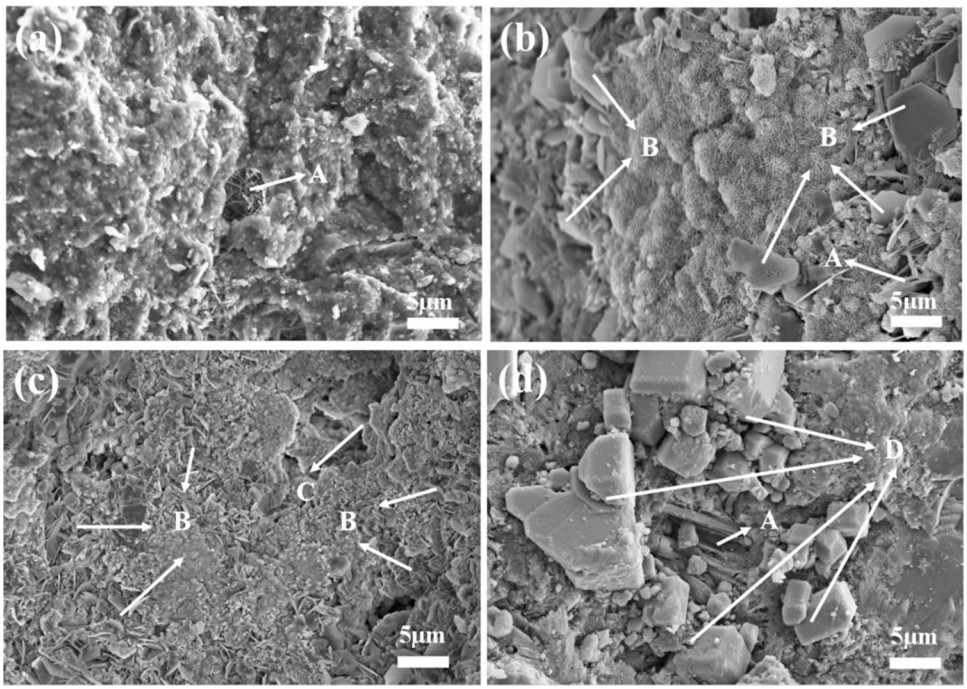

Fig. 8 SEM images of different samples. where, *A*: ettringite; B: Friedel's salt; C: C-S–H gel; and D: NaCl and KCl

also be observed, ensuring a denser microstructure and higher compressive strength for the backfill material. For sample M40 (arrow in Fig. 8d), in addition to the generated hydration products, the sample surface was covered by a large amount of NaCl and KCl particles (D) due to excessive Cl^- from MSWI FA (Qian et al. 2008).

Conclusion

In this study, feasibility of using GBFS and FGDG to solidify MSWI FA to prepare cement-free backfill material was examined. Results indicated that without adding cement or other alkaline activators, OH^- in MSWI FA activated the potential activity of GBFS, triggering the hydration reaction. This reaction resulted in the use of solid waste to solidify harmful substances in MSWI FA, providing a new method for MSWI FA disposal. This method was also found to be very cost effective for mine backfill. It was found that an appropriate amount of MSWI FA (i.e., 20 and 30 wt%) in backfill material improved its mechanical strength, fluidity and rheological properties, as well as reduced its setting time and ratio of bleeding while restraining drying shrinkage. When MSWI FA content was > 40%, internal homogeneity of the backfill material was poor due to its strong water absorption, producing viscous mortar and reducing the aforementioned workability of the backfill material. An MSWI FA dosage of 30% resulted in the optimum performance of the backfill material. Its compressive strength was 25.69 MPa after 28d curing, fluidity was 284 mm, and the final shrinkage rate was 9.31×10^{-5}%; the final bleeding rate reached 0.26% after 187 min. Water content of standard consistency in sample M30 (19.8%) was the lowest among all samples, and the initial and final setting times were 2.9 and 3.7 h, respectively. In the rheological performance test, plastic viscosity of sample M30 was 1.70; shear stress and yield stress reached 275.70 Pa and 64.99 Pa, respectively. In addition, the concentration of heavy metal leaching was lower than the relevant safety standard.

The hydration characteristics of pastes were analyzed by XRD, FTIR and SEM. Results indicated that for sample M10, insufficient MSWI FA incorporation resulted in the formation of a low amount of ettringite by the hydration reaction of SO_4^{2-} from FGDG and $[Ca_2Al(OH)_6 \cdot 2H_2O]^+$ from GBFS. When MSWI FA was added, the alkaline environment improved the GBFS activity, the hydration reaction was favored by Cl^- from MSWI FA, and ettringite and Friedel's salt co-existed in the cementitious system. With a further increase in MSWI FA content, almost all $[Ca_2Al(OH)_6 \cdot 2H_2O]^+$ released by GBFS reacted with Cl^- rather than SO_4^{2-} to produce Friedel's salt while ettringite disappeared. However, when the MSWI FA content reached 40%, NaCl and KCl from MSWI FA were also identified on the surface of backfill material due to an excessive amount of Cl^-.

Results from this investigation indicate that mine backfill material prepared using MSWI FA as cementitious material to activate GBFS has a good level of performance. A large volume of hydration products were also generated. This method provides a low cost and superior performance for cement-free mine backfill material.

Supplementary Information The online version contains supplementary material available at https://doi.org/10.1007/s13762-022-04138-3.

Acknowledgements We appreciate the financial support of the Science and Technology Department of Hebei Province, China [18273807D] and the language assistance from Gang Zhang of MogoEdit.

Authors contribution KW was involved in the formal analysis, investigation; validation, methodology and writing—original draft; WN contributed to the resources and supervision; KL contributed to the funding acquisition and writing—review and editing; XH was involved in the investigation and validation.

Availability of data and material The datasets used or analyzed during the current study are available from the corresponding author upon reasonable request.

Code availability Not applicable.

Declarations

Conflict of interest The authors declare that they have no competing interests.

Ethics approval and consent to participate Not applicable.

Consent for publication Written informed consent for publication was obtained from all participants.

References

Behera SK, Ghosh CN, Mishra DP, Singh P, Mishra K, Buragohain J, Mandal PK (2020) Strength development and microstructural investigation of lead-zinc mill tailings based paste backfill with fly ash as alternative binder. Cement Concr Compos 109:103553

Bie R, Chen P, Song X, Ji X (2016) Characteristics of municipal solid waste incineration fly ash with cement solidification treatment. J Energy Inst 89:704–712

Cihangir F, Ercikdi B, Kesimal A, Turan A, Deveci H (2012) Utilisation of alkali-activated blast furnace slag in paste backfill of high-sulphide mill tailings: Effect of binder type and dosage. Miner Eng 30:33–43

Clavier KA, Watts B, Liu Y, Ferraro CC, Townsend TG (2019) Risk and performance assessment of cement made using municipal solid waste incinerator bottom ash as a cement kiln feed. Resour Conserv Recycl 146:270–279

Deng Y, Peng P, Jia L, Yin H, Hu J, Mao W (2020) Atmospheric bulk deposition of polychlorinated dibenzo-p-dioxins and dibenzofurans (PCDD/Fs) in the vicinity of MSWI in Shanghai, China. Ecotoxicol Environ Saf 196:110493

Erfanimanesh A, Sharbatdar MK (2020) Mechanical and microstructural characteristics of geopolymer paste, mortar, and concrete containing local zeolite and slag activated by sodium carbonate. J Build Eng 32:101781

Fan Z, Men J, Gong C, Liu Y (2018) Experimental study on proportioning of unclassified tailings paste based on requirements of high strength backfill body. J Saf Sci Technol 14:102–106

Fan C, Wang B, Ai H, Qi Y, Liu Z (2021a) A comparative study on solidification/stabilization characteristics of coal fly ash-based geopolymer and Portland cement on heavy metals in MSWI fly ash. J Clean Prod 319:128790

Fan C, Wang B, Qi Y, Liu Z (2021b) Characteristics and leaching behavior of MSWI fly ash in novel solidification/stabilization binders. Waste Manag 131:277–285

Ghourchian S, Wyrzykowski M, Lura P (2016) The bleeding test: a simple method for obtaining the permeability and bulk modulus of fresh concrete. Cem Concr Res 89:249–256

Hatami AM, Sabour MR, Nikravan M (2021) A systematic analysis of research trends on incineration during 2000–2019. Int J Environ Sci Technol 18:353–364

He H, Lu S, Peng Y, Tang M, Zhan M, Lu S, Xu L, Zhong W, Xu L (2022) Emission characteristics of dioxins during iron ore Co-sintering with municipal solid waste incinerator fly ash in a sintering pot. Chemosphere 287:131884

Huang X, Zhuang RL, Muhammad F, Yu L, Shiau YC, Li D (2017) Solidification/stabilization of chromite ore processing residue using alkali-activated composite cementitious materials. Chemosphere 168:300–308

Igor C, Maria H, Carmen T, Nicolina ID (2018) Synthesis and characterisation of a binder cement replacement based on alkali activation of fly ash waste. Process Saf Environ Prot 119:23–35

Jiang H, Mamadou F, Liang C (2016) Yield stress of cemented paste backfill in sub-zero environments: experimental results. Miner Eng 92:141–150

Jiang G, Wu A, Wang Y, Li J (2019) The rheological behavior of paste prepared from hemihydrate phosphogypsum and tailing. Constr Build Mater 229:116870

Jin M, Zheng Z, Sun Y, Chen L, Jin Z (2016) Resistance of metakaolin-MSWI fly ash based geopolymer to acid and alkaline environments. J Non-Cryst Solids 450:116–122

Lee T-C, Wang W-J, Shih P-Y, Lin K-L (2009) Enhancement in early strengths of slag-cement mortars by adjusting basicity of the slag prepared from fly-ash of MSWI. Cem Concr Res 39:651–658

Li D, Guo X, Tian Q, Xu Z, Xu R, Zhang L (2017) Synthesis and application of Friedel's salt in arsenic removal from caustic solution. Chem Eng J 323:304–311

Li J, Zhang S, Wang Q, Ni W, Li K, Fu P, Hu W, Li Z (2020) Feasibility of using fly ash–slag-based binder for mine backfilling and its associated leaching risks. J Hazard Mater 400:123191

Liu X, Zhao X, Yin H, Chen J (2018) Intermediate-calcium based cementitious materials prepared by MSWI fly ash and other solid wastes: hydration characteristics and heavy metals solidification behavior. J Hazard Mater 349:262–271

Liu J, Hu L, Tang L, Ren J (2021) Utilisation of municipal solid waste incinerator (MSWI) fly ash with metakaolin for preparation of alkali-activated cementitious material. J Hazard Mater 402:123451

Long W-J, Peng J-K, Gu Y-C, Li J-L, Dong B, Xing F, Fang Y (2021) Recycled use of municipal solid waste incinerator fly ash and ferronickel slag for eco-friendly mortar through geopolymer technology. J Clean Prod 307:127281

Men R, Xie C (2018) Numerical and experimental study on proportion of paste filling slurry with full tailings. Min Res Dev 38:28–31

Nguyen Q, Boger D (1985) Thixotropic behaviour of concentrated bauxite residue suspensions. Rheol Acta 24:427–437

Petra VL, David VB (1996) Yield stress measurements with the vane. J Non-Newton Fluid Mech 63:235–261

Qian GR, Shi J, Cao YL, Xu YF, Chui PC (2008) Properties of MSW fly ash-calcium sulfoaluminate cement matrix and stabilization/solidification on heavy metals. J Hazard Mater 152:196–203

Ren P, Ling T-C (2021) Roles of chlorine and sulphate in MSWIFA in GGBFS binder: Hydration, mechanical properties and stabilization considerations. Environ Pollut 284:117175

Ren J, Hu L, Dong Z, Tang L, Xing F, Liu J (2021) Effect of silica fume on the mechanical property and hydration characteristic of alkali-activated municipal solid waste incinerator (MSWI) fly ash. J Clean Prod 295:126317

Shao N, Wei X, Monasterio M, Dong Z, Zhang Z (2021) Performance and mechanism of mold-pressing alkali-activated material from MSWI fly ash for its heavy metals solidification. Waste Manag 126:747–753

Shi Z, Geiker MR, Lothenbach B, De Weerdt K, Garzón SF, Enemark-Rasmussen K, Skibsted J (2017) Friedel's salt profiles from thermogravimetric analysis and thermodynamic modelling of Portland cement-based mortars exposed to sodium chloride solution. Cement Concr Compos 78:73–83

Sobiecka E (2013) Investigating the chemical stabilization of hazardous waste material (fly ash) encapsulated in Portland cement. Int J Environ Sci Technol 10:1219–1224

Šyc M, Simon FG, Hykš J, Braga R, Biganzoli L, Costa G, Funari V, Grosso M (2020) Metal recovery from incineration bottom ash: State-of-the-art and recent developments. J Hazard Mater 393:122433

Tan WF, Wang LA, Huang C, Green JE (2013) Municipal solid waste incineration fly ash sintered lightweight aggregates and kinetics model establishment. Int J Environ Sci Technol 10:465–472

Tang P, Chen W, Xuan D, Zuo Y, Poon CS (2020) Investigation of cementitious properties of different constituents in municipal solid waste incineration bottom ash as supplementary cementitious materials. J Clean Prod 258:120675

Tian X, Rao F, León-Patiño CA, Song S (2021) Co-disposal of MSWI fly ash and spent caustic through alkaline-activation consolidation. Cement Concr Compos 116:103888

Wan S, Zhou X, Zhou M, Han Y, Chen Y, Geng J, Wang T (2018) Hydration characteristics and modeling of ternary system of municipal solid wastes incineration fly ash-blast furnace slag-cement. Constr Build Mater 180:154–166

Wang L, Jamro IA, Chen Q, Li S (2015) Immobilization of trace elements in municipal solid waste incinerator (MSWI) fly ash by producing calcium sulphoaluminate cement after carbonation and washing. Waste Manag 34:184

Wang K, Ni W, Zhang S (2019) Stabilization/solidfication of cadmium in municipal solid waste incineration fly ash by using cemented backfill agent. In: 2018 International conference on civil, architecture and disaster prevention China

You N, Liu Y, Gu D, Ozbakkaloglu T (2020) Rheology, shrinkage and pore structure of alkali-activated slag-fly ash mortar incorporating copper slag as fine aggregate. Constr Build Mater 242:118029

Yu Z, Zhao Y, Ba H, Liu M (2021) Relationship between buck electrical resistivity and drying shrinkage in cement paste containing expansive agent and mineral admixtures. J Build Eng 39:102261

Zhan X, Wang LA, Wang L, Wang X, Gong J, Yang L, Bai J (2019) Enhanced geopolymeric co-disposal efficiency of heavy metals from MSWI fly ash and electrolytic manganese residue using complex alkaline and calcining pre-treatment. Waste Manag 98:135–143

Zhang L, Ahmari S, Zhang J (2011) Synthesis and characterization of fly ash modified mine tailings-based geopolymers. Constr Build Mater 25:3773–3781

Zhang J, Shi C, Zhang Z (2019a) Chloride binding of alkali-activated slag/fly ash cements. Constr Build Mater 226:21–31

Zhang Y, Zhang S, Ni W, Yan Q (2019b) Immobilisation of high-arsenic-containing tailings by using metallurgical slag-cementing materials. Chemosphere 223:117–123

Zheng L, Gao X, Wang W, Li Z (2019) Utilization of MSWI fly ash as partial cement or sand substitute with focus on cementing efficiency and health risk assessment. Front Environ Sci Eng 14:84–94

Zhou X, Zhou M, Wu X, Han Y, Geng J, Wang T, Wan S, Hou H (2017) Reductive solidification/stabilization of chromate in municipal solid waste incineration fly ash by ascorbic acid and blast furnace slag. Chemosphere 182:76–84